PHYSICAL REVIEW B VOLUME 59, NUMBER 4 15 JANUARY 1999-II

In situ XPS analysis of various iron oxide films grown by NO_2-assisted molecular-beam epitaxy

T. Fujii,* F. M. F. de Groot, and G. A. Sawatzky
Department of Solid State Physics, Materials Science Centre, University of Groningen, Nijenborgh 4, 9747AG Groningen, The Netherlands

F. C. Voogt and T. Hibma
Department of Physical Chemistry, Materials Science Centre, University of Groningen, Nijenborgh 4, 9747AG Groningen, The Netherlands

K. Okada
Department of Physics, Faculty of Science, Okayama University, Tsushima-naka 3-1-1, Okayama 700-0082, Japan

(Received 27 July 1998)

We report on a systematic analysis of x-ray photoelectron spectroscopy (XPS) core- and valence-level spectra of clean and well-characterized iron oxide films, i.e., α-Fe_2O_3, γ-Fe_2O_3, $Fe_{3-\delta}O_4$, and Fe_3O_4. All iron oxide films were prepared epitaxially by NO_2-assisted molecular-beam epitaxy on single crystalline MgO(100) and α-Al_2O_3(0001) substrates. The phase and stoichiometry of the films were controlled precisely by adjusting the NO_2 pressure during growth. The XPS spectrum of each oxide clearly showed satellite structures. These satellite structures were simulated using a cluster-model calculation, which could well reproduce the observed structures by considering the systematic changes in both the Fe $3d$ to O $2p$ hybridization and the d-d electron-correlation energy. The small difference in the satellite structures between α-Fe_2O_3 and γ-Fe_2O_3 resulted mainly from changes in the Fe-O hybridization parameters, suggesting an increased covalency in γ-Fe_2O_3 compared to α-Fe_2O_3. With increasing reduction in the γ-Fe_2O_3-Fe_3O_4 system, the satellite structures in XPS became unresolved. This was not only due to the formation of Fe^{2+} ions, but also to nonhomogeneous changes in the hybridization parameters between octahedral and tetrahedral Fe^{3+} ions.
[S0163-1829(99)02704-6]

I. INTRODUCTION

The electronic structure of iron oxides has been the subject of many experimental and theoretical studies.[1–11] Iron oxides are materials of great importance in many technological applications such as catalysts and magnetic devices. Furthermore, they are products in the corrosion process of steel.[12] To obtain information about the electronic structure of solids, x-ray photoelectron spectroscopy (XPS) is one of the most powerful tools.[1–6] Despite extensive XPS investigations of various iron oxides, to our knowledge a complete systematic understanding of their electronic structures has not yet been achieved. The difficulty in interpreting XPS spectra arises from both theoretical and experimental facts. The theoretical difficulty comes from the correlation effects among the Fe $3d$ electrons and the hybridization between the Fe $3d$ and the ligand O $2p$ states, which give complicated multiplet structures in the spectra. The experimental one is associated with controlling the stoichiometry of iron oxides and with preparing clean and well-characterized surfaces. XPS spectra are easily influenced by the presence of contaminations such as water and hydrocarbons on the surface.

The possibility to grow well-crystallized iron-oxide films by molecular beam epitaxy (MBE) has been widely demonstrated.[13–20] In the MBE growth of iron-oxide films, the use of NO_2 as a source of oxygen allows the formation of almost all iron oxide phases in the Fe-O system. The stoichiometry of the oxides can be controlled precisely by adjusting the flux of NO_2. Depending on the NO_2 pressure during the growth, epitaxial layers of stoichiometric Fe_3O_4 (magnetite) or all phases of nonstoichiometric $Fe_{3-\delta}O_4$ up to the completely oxidized one, i.e., stoichiometric γ-Fe_2O_3 (maghemite), can be formed on cubic MgO(100) substrates,[18] while on hexagonal α-Al_2O_3 substrates in combination with the high NO_2 pressure, epitaxial layers of stoichiometric α-Fe_2O_3 (hematite) are formed.[19] Therefore, we will report here on *in situ* XPS measurements on clean and well-characterized surfaces of various iron oxide films, prepared by the NO_2-assisted MBE technique.

The crystal structures of these oxides are normally described as structures based upon a framework of close-packed (cp) oxygen sublattices. Hematite is an antiferromagnetic insulator with a corundum structure, in which Fe^{3+} ions are octahedrally coordinated by hexagonal cp O^{2-} ions. Magnetite, maghemite, and their intermediate compound, $Fe_{3-\delta}O_4$, are ferrimagnetic materials having an inverse spinel structure with cubic cp O^{2-} ions. The usual formula representation of magnetite is $[Fe^{3+}]_{tet}[Fe^{2+}Fe^{3+}]_{oct}O_4$, indicating that the Fe^{2+} ions occupy octahedral sites and that the Fe^{3+} ions are distributed evenly over octahedral and tetrahedral sites. At room temperature, Fe_3O_4 has a high conductivity because of a rapid electron hopping between octahedral Fe^{2+} and Fe^{3+} ions. Oxidizing Fe_3O_4 to $Fe_{3-\delta}O_4$, the Fe^{2+} ions in the octahedral sites are replaced with vacancies and Fe^{3+} ions as $[Fe^{3+}]_{tet}[Fe_{1-3\delta}{}^{2+}Fe_{1+2\delta}{}^{3+}\square_{\delta}]_{oct}O_4$. γ-Fe_2O_3, which is the insulator, has the highest oxidized structure of $[Fe^{3+}]_{tet}[Fe_{5/3}{}^{3+}\square_{1/3}]_{oct}O_4$.

It is well known that XPS spectra of iron oxides exhibit so-called shake-up satellite structures. These satellite structures, which are very sensitive to the electronic structure of the compounds, are frequently used as fingerprints to identify the iron oxide phases. Theoretically, the cluster-model calculation can successfully be applied to reproduce the structures in XPS spectra of $3d$ transition compounds.[6,21–24] The multiplet interaction of the core hole created in the photoemission process with the $3d$ electrons is strong enough to redistribute the final-state electron configurations. Also, the configuration interaction produced by charge transfer from the ligand $2p$ orbitals to the metal $3d$ states influences the shape of the spectrum. In this paper, we present the systematic study of XPS Fe $2p$ core-level and valence-band spectra of various epitaxial iron-oxide films, based upon this theory.

II. EXPERIMENT

To prepare various iron oxides as epitaxial films, we used an ultrahigh vacuum (UHV) system comprising both MBE and XPS chambers. The base pressure of the MBE chamber was 1×10^{-8} Pa. Before deposition, a single-crystalline substrate of MgO(100) or α-Al_2O_3(0001) with dimensions of $10\times10\times0.3\sim1.0\,mm^3$ was annealed for 12 h at 923 K under an O_2 pressure of 1×10^{-4} Pa, in order to remove hydrocarbon contaminations from the surface. Crystalline order and cleanliness of the substrate surface were checked with low-energy electron diffraction (LEED), reflection high-energy electron diffraction (RHEED), Auger electron spectroscopy, and XPS.

During deposition, Fe metal was evaporated from a Knudsen cell onto the substrates, with the simultaneous oxidization by an NO_2 flux coming from a small buffer volume. The flux was regulated by adjusting the pressure in the buffer volume, and therewith the degree of oxidation could be precisely controlled. By using a small flux of the more reactive NO_2, instead of conventional O_2, the MBE chamber could maintain a low-background pressure ($<1\times10^{-5}$ Pa) during deposition. The substrate temperature was fixed at 623 K for α-Fe_2O_3 films on α-Al_2O_3 or at 523 K for Fe_3O_4, $Fe_{3-\delta}O_4$, and γ-Fe_2O_3 films on MgO. All films had a thickness of about 250 Å, which was monitored by counting the number of RHEED intensity oscillations and by a quartz-crystal oscillator. The δ values of $Fe_{3-\delta}O_4$ films on MgO were determined *ex situ* by conversion-electron Mössbauer spectroscopy (CEMS). Figures 1(a) and 1(b) are typical CEMS spectra of $Fe_{3-\delta}O_4$ films prepared at NO_2 buffer volume pressure of 0.166 and 1.33 Pa, respectively. The spectrum at $NO_2=0.166$ Pa corresponds to nearly stoichiometric Fe_3O_4, while the spectrum at 1.33 Pa was consistent with the one for stoichiometric γ-Fe_2O_3. The δ values of all $Fe_{3-\delta}O_4$ sample films are summarized in Table I as a function of the NO_2 pressure. We emphasize here that the NO_2-assisted MBE technique could successfully induce the formation of a stoichiometric film of the metastable spinel oxide, γ-Fe_2O_3. Details of the thin-film growth process, stoichiometry determination, and crystalline structure of these films were already reported in Refs. 15 and 18–20.

After deposition, the sample films were immediately transferred from the MBE chamber to the XPS chamber under UHV conditions. XPS was performed by using non-

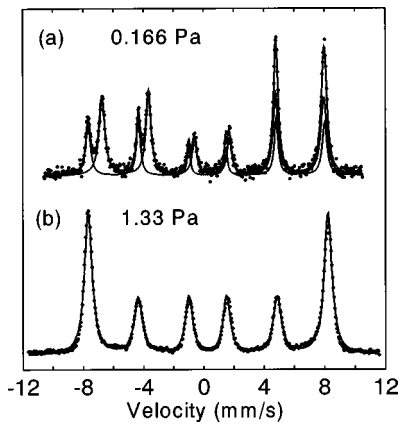

FIG. 1. Typical CEMS spectra of $Fe_{3-\delta}O_4$ films grown on MgO(100) at NO_2 buffer volume pressures of (a) 0.166 Pa and (b) 1.33 Pa.

monochromatic Al Kα radiation ($h\nu=1486.6$ eV) and a VG Clam II hemispherical electron-energy analyzer. The pressure of the XPS chamber during the measurement was 5×10^{-9} Pa, and the instrumental broadening measured at the Ag Fermi edge was estimated to be about 1 eV. Some sample films showed charging (<8 eV) in XPS spectra because of their insulator nature. The binding energies were corrected for the charging effect by assuming a constant binding energy for the O 1*s* peak of 530.1 eV.[1] All spectra were corrected by subtracting a Shirley-type background,[25] after subtracting the satellites due to the K$\alpha_3\alpha_4$ components of the incident x-rays. The XPS O 1*s* spectra of the sample films, shown in Fig. 2, all had a nearly identical single-line profile. The symmetric peak shape without low-intensity side bands proves the cleanliness of the surfaces.

III. CALCULATION METHOD

In the cluster model approach to simulate XPS spectra of $3d$ transition-metal compounds, the parameters of the Coulomb interaction (Q) between the core hole ($\underline{c}$) and the $3d$ electron, the correlation energy (U) between the $3d$ electrons, the ligand $2p$ to the metal $3d$ charge-transfer energy (Δ), and the ligand $2p$ to the metal $3d$ hybridization energy (T) are explicitly taken into account.[21,24] The ground-state electron configuration is given by a linear combination of $3d^n$, $3d^{n+1}\underline{L}$, and $3d^{n+2}\underline{L}^2$ up to $3d^{10}\underline{L}^{10-n}$, where n and $\underline{L}$ denote the number of $3d$ electrons and the ligand hole on

TABLE I. The δ values in $Fe_{3-\delta}O_4$ films determined by *ex situ* conversion electron Mössbauer spectroscopy, as a function of the NO_2 buffer volume pressure during deposition.

NO_2 buffer volume pressure (Pa)	δ values in $Fe_{3-\delta}O_4$
0.166	0.013 ± 0.004
0.233	0.030 ± 0.004
0.333	0.251 ± 0.007
0.400	0.270 ± 0.006
0.666	0.284 ± 0.008
1.33	0.333

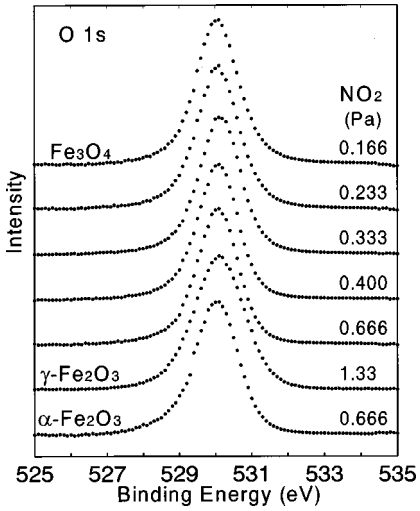

FIG. 2. XPS O 1(s) core-level spectra of various iron-oxide films prepared by the NO_2-assisted MBE technique. The NO_2 buffer volume pressures during deposition are indicated in each spectrum.

ligand O^{2-} ions, respectively. In our calculations, the higher energy terms beyond the first three configurations were neglected. In the same way, the final-state configuration in XPS is given by a linear combination of $\underline{c}3d^n$, $\underline{c}3d^{n+1}\underline{L}$, and $\underline{c}3d^{n+2}\underline{L}^2$. The core-hole potential lowers the $3d^{n+1}\underline{L}$ and $3d^{n+2}\underline{L}^2$ states by Q and $2Q$, respectively, compared to the $3d^n$ state, which causes a different ordering of final-state levels from initial ones. This is the reason for the strong satellite structure in XPS spectra.[26,27]

In the simplest crystal-field picture, the $3d$ levels in octahedral symmetry (O_h) are split into two e_g and three t_{2g} orbitals, separated by $10Dq$. Each orbital gives a different p-d hybridization energy, as $Te_g = \sqrt{3}(pd\sigma)$ or $Tt_{2g} = 2(pd\pi)$, defined by the Slater-Koster transfer integrals.[28] The tetrahedral symmetry (T_d) gives, compared to the O_h symmetry, an inverted crystal-field splitting.[27] Here, the two e orbitals are lower in energy than the three t_2 orbitals. The p-d hybridization for each orbital is defined as $Te = 2/3\sqrt{6}(pd\pi)$ or $Tt_2 = 2/3\sqrt{2}(pd\pi)$-$2/3\sqrt{3}(pd\sigma)$. In the present calculation, Δ and U were defined with respect to the center of gravity of the configuration. Only three parameters of Δ, U, and $Te_{(g)}$ were treated as adjustable parameters for simplicity. The anisotropy in hybridization was taken into account, adopting the empirical relation $Te_g = -2Tt_{2g}$ and $Te = -1/2\,Tt_2$.[29] In the XPS Fe $3d$ valence-band spectra, the $3d$ electron hole is created in the Fe $3d$ valence shell. The Coulomb interaction between the $3d$ valence hole and the $3d$ electron was considered equal to U. While in the XPS Fe $2p$ core-level spectra, the Coulomb interaction (Q) was assumed to be slightly (0.5 eV) larger than U. Because a full-multiplet interatomic charge-transfer model approves the larger U value than that the conventional relation of $U = 0.8Q$ expected, which is originally proposed by a pure charge-transfer model.[30] If we adopted the relation of $U = 0.8Q$, we could not reproduce the XPS Fe $3d$ valence-band and Fe $2p$ core-level spectra simultaneously by using the same parameter values. The value of $10Dq$ is effected by both the ionic and the covalent contribution. The latter can be estimated from the short-range model parameters as $10Dq(\mathrm{cov}) = \sqrt{\Delta^2 + 4Te_g^2} - \sqrt{\Delta^2 + 4Tt_{2g}^2}$.[31] The former was fixed to $10Dq(\mathrm{ion}) = 0.5$ eV because it had little effect on the XPS spectral shape.[24] The Slater integrals were scaled down to 85% of the ionic Hartree-Fock-Slater calculation.

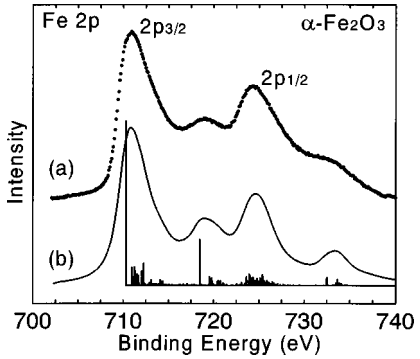

FIG. 3. Observed (a) and simulated (b) XPS Fe $2p$ core-level spectra of an α-Fe_2O_3(0001) film on α-Al_2O_3(0001). The parameter values used for the simulation are listed in Table II.

IV. RESULTS AND DISCUSSION

A. α-Fe_2O_3 and γ-Fe_2O_3 films

Ferric oxides are polymorphic, i.e., they occur as α-Fe_2O_3 with a corundum structure and γ-Fe_2O_3 with a deficient spinel structure. Despite the large differences in their crystal structures, the XPS Fe $2p$ core-level spectra of α-Fe_2O_3 and γ-Fe_2O_3 are known to be almost identical with each other.[2] Figure 3(a) shows the XPS Fe $2p$ spectrum of an α-Fe_2O_3 film on α-Al_2O_3(0001), while the spectrum of a γ-Fe_2O_3 film on MgO(100) is shown in Fig. 4(a). The formation of stoichiometric γ-Fe_2O_3 without any Fe^{2+} components was confirmed by CEMS, RHEED and LEED. The Fe $2p_{3/2}$ and $2p_{1/2}$ main peaks of both films are clearly accompanied by satellite structures on their high binding-energy side, at about 8 eV. The binding energy of about 711 eV for the Fe $2p_{3/2}$

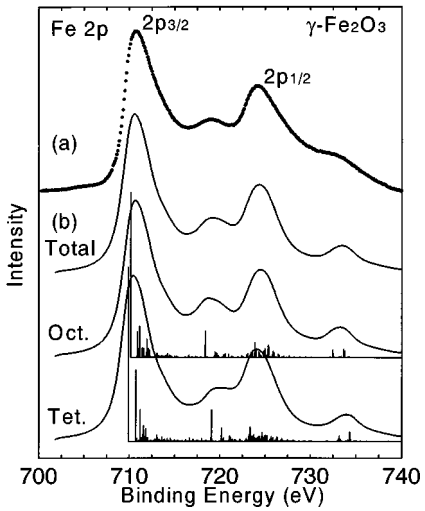

FIG. 4. Observed (a) and simulated (b) XPS Fe $2p$ core-level spectra of a γ-Fe_2O_3(100) film on MgO(100). The simulated spectrum labeled ''Total'' is obtained by a weighted summation of the octahedral and tetrahedral Fe^{3+} components. The parameter values used for the simulation are listed in Table II.

TABLE II. Spectral parameters of the XPS Fe $2p_{3/2}$ core-level spectra of α-Fe_2O_3 and γ-Fe_2O_3 films shown in Figs. 3(a) and 4(a), respectively. Tabulated are the binding energy of the $2p_{3/2}$ main peak maximum (BE), the intensity ratio of the satellite to the main peak (I_S/I_M), and the separation between them (δE).

Compound	BE (eV)	I_S/I_M	δE (eV)
α-Fe_2O_3	710.9	0.473	8.1
γ-Fe_2O_3	710.7	0.446	8.2

main peak is consistent with typical values for the ferric oxides reported in the literature.[1–4] The observed spectral parameters of the $2p_{3/2}$ peaks for both films are listed in Table II. We find that the XPS Fe $2p$ spectrum of the clean γ-Fe_2O_3 film have two remarkable features compared with that of the clean α-Fe_2O_3, and both are quite reproducible: (i) the intensity of the satellite peak is reduced, and (ii) the $2p_{3/2}$ main peak is slightly shifted to lower binding energy.

In the case of α-Fe_2O_3, all the Fe^{3+} ions occupy octahedral sites. So, the calculation of the XPS Fe $2p$ core-level spectrum for α-Fe_2O_3 involved only one FeO_6 cluster. Figure 3(b) shows a simulated XPS Fe $2p$ spectrum by using the parameter values listed in Table III. The simulated spectrum well reproduces the satellite structures in the observed spectrum. The parameter values used agree well with the values reported by other groups, as measured with XPS (Ref. 6) or x-ray absorption spectroscopy.[11] It should be noticed that ''$\Delta_{\rm eff}$'' and ''$U_{\rm eff}$'' as used in the so-called Zaanen-Sawatzky-Allen (ZSA) diagram[26] are defined with respect to the lowest energy configuration by both the multiplet splitting and the crystal-field splitting. The effective charge-transfer energy $\Delta_{\rm eff}$ and the $3d$-$3d$ correlation energy $U_{\rm eff}$ have the following relations with ''Δ'' and ''U'' used in our calculation, i.e., $\Delta_{\rm eff}=\Delta+2\delta d^n-\delta d^{n+1}-\delta d^n\underline{L}$ and $U_{\rm eff}=U+2\delta d^n-\delta d^{n+1}-\delta d^{n-1}$, respectively, where δd^n denotes the energy difference between the center of gravity and the lowest energy for the d^n configuration. Depending on the relative values of $U_{\rm eff}$ and $\Delta_{\rm eff}$, the oxides are classified as a Mott-Hubbard insulator ($U_{\rm eff}<\Delta_{\rm eff}$) or a charge-transfer insulator ($U_{\rm eff}>\Delta_{\rm eff}$). The parameter values in Table III are plotted in the ZSA diagram shown in Fig. 5. The electronic structure in the α-Fe_2O_3 film is clearly that of a charge-transfer insulator as reported previously.[6,11]

TABLE III. Parameter values (Δ, $Te_{(g)}$, $Tt_{2(g)}$, U, and Q) of various iron oxides used for the cluster calculation of the XPS Fe $2p$ spectra. The last column is the iron-to-oxygen mean distance (r) of each site reported for bulk crystals.

Compound	Sites	Δ (eV)	$Te_{(g)}$ (eV)	$Tt_{2(g)}$ (eV)	U (eV)	Q (eV)	r (Å)
α-Fe_2O_3	Fe_{Oct}^{3+}	2.0	2.6	−1.3	7.5	8.0	1.99
γ-Fe_2O_3	Fe_{Oct}^{3+}	2.0	2.7	−1.35	7.0	7.5	2.03
	Fe_{Tet}^{3+}	2.0	1.35	−2.7	7.0	7.5	1.89
Fe_3O_4	Fe_{Oct}^{3+}	2.0	2.2	−1.1	7.5	8.0	2.07
	Fe_{Oct}^{2+}	4.0	2.3	−1.15	7.0	7.5	2.07
	Fe_{Tet}^{3+}	2.0	1.35	−2.7	7.0	7.5	1.87

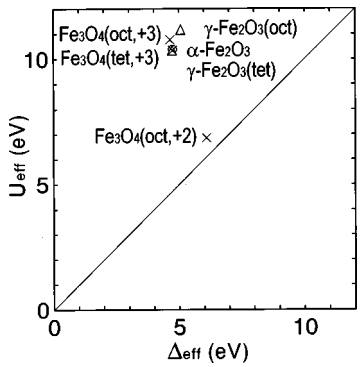

FIG. 5. Zaanen-Sawatzky-Allen diagram for the various iron oxides: ○, α-Fe_2O_3, △, γ-Fe_2O_3; and ×, Fe_3O_4.

In γ-Fe_2O_3, the Fe^{3+} ions occupy both octahedral and tetrahedral sites with unequal frequency of 5:3. Strictly speaking, the octahedral sites in γ-Fe_2O_3 consist of three different sites because of the small distortions from the perfect octahedron. However, the electronic structures of these pseudo-octahedral sites were reported to be quite similar to each other.[11] Thus, our XPS calculation for γ-Fe_2O_3 involved only one octahedral and one tetrahedral cluster, ignoring the pseudo-octahedral structures. The simulated XPS Fe $2p$ spectrum of γ-Fe_2O_3 shown in Fig. 4(b) was obtained by weighted summation of the octahedral Fe^{3+} and the tetrahedral Fe^{3+} components. The problem at this point is the relative energy position between them. We assumed that the centers of gravity of the ground- and final-state energy levels for each site ions are the same. The binding energy of the Fe $2p_{3/2}$ main peak for the tetrahedral sites is slightly lowered from that for the octahedral sites, even though both sites have the same energy levels of the center of gravity. This could be one of the reasons for the lowered binding energy of the Fe $2p_{3/2}$ main peak for the γ-Fe_2O_3 film. The inverted crystal field in the tetrahedral ions gives different $\Delta_{\rm eff}$ and $U_{\rm eff}$ from the octahedral ones. But the insulating gaps of $\Delta_{\rm eff}$ and $U_{\rm eff}$ in both sites of γ-Fe_2O_3 hardly differ from those in α-Fe_2O_3. It certainly is a charge-transfer insulator as shown in the ZSA diagram of Fig. 5.

It is well known that the p-d hybridization considerably effects the satellite intensities.[19,21–24,27] For theoretical simplicity, we considered here only two ground-state configurations, i.e., d^5 and $d^6\underline{L}$, and disregarded the multiplet splitting. The ground state is written as $\psi_i=\cos\alpha|d^5\rangle+\sin\alpha|d^6\underline{L}\rangle$, where α is the coefficient proportional to T/Δ in the weak hybridization limit. The final state forms bonding and antibonding combinations. The main peak corresponds to the transition from the ground state to the bonding final state, written as $\psi_f=\sin\beta|\underline{c}d^5\rangle+\cos\beta|\underline{c}d^6\underline{L}\rangle$, while the satellite peak is due to the antibonding state written as $\psi_f^*=-\cos\beta|\underline{c}d^5\rangle+\sin\beta|\underline{c}d^6\underline{L}\rangle$, with β the coefficient proportional to $T/(Q\text{-}\Delta)$. Then, the main and the satellite peaks are normally assigned to the transition to the ''screened'' core-hole final state ($|\underline{c}d^6\underline{L}\rangle$) and the ''unscreened'' final state ($|\underline{c}d^5\rangle$), respectively, when $Q>\Delta$.[27] The intensity of the satellite peak is given by the transition-matrix elements between ψ_i and ψ_f^*, which are approximately written as $1\text{-}T^2/\Delta(Q\text{-}\Delta)$. It follows that the satellite intensity is strongly influenced by T. The other parameters Δ and Q can-

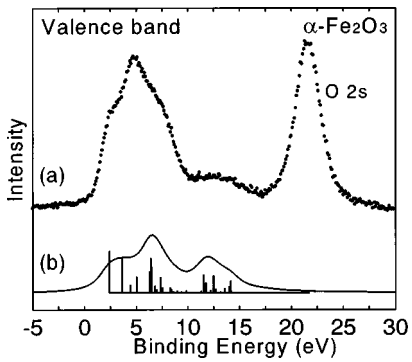

FIG. 6. Observed (a) and simulated (b) XPS spectra of the valence-band region of an α-Fe_2O_3(0001) film. The simulated spectrum includes only Fe $3d$ derived states and excludes nonbonding O $2p$ states. The parameter values measured in the XPS Fe $2p$ spectrum (Fig. 3) are used for the simulation.

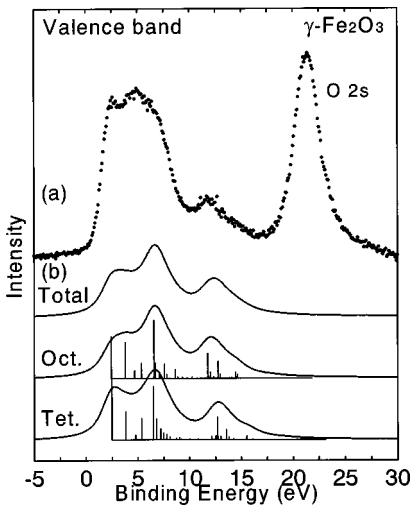

FIG. 7. Observed (a) and simulated (b) XPS spectra of the valence-band region of a γ-Fe_2O_3(100) film on MgO(100). The parameter values measured in the XPS Fe $2p$ spectrum (Fig. 4) are used for the simulation. The simulated spectrum labeled ''Total'' is obtained by a weighted summation of the octahedral and tetrahedral Fe^{3+} components.

not reasonably reproduce the simultaneous changes in both the satellite intensities and the positions. Therefore, we conclude that the decreased satellite intensity of γ-Fe_2O_3 compared to α-Fe_2O_3 is mainly caused by an increase in T. However, the Harrison's relation states that T varies with the interatomic distance as $r^{-3.5}$.[29] So one expects, on the contrary, a decrease in T of γ-Fe_2O_3, because the octahedral Fe-O distance in bulk γ-Fe_2O_3 is about 2% larger than that in bulk α-Fe_2O_3.[32] Therefore, our experimental results suggest that the Harrison's relations could not be applied rigidly on these systems because the crystal structures of γ-Fe_2O_3 and α-Fe_2O_3 are very different. Another explanation might be that the lattice mismatch between the film and substrate induces anisotropic strains at the interface,[33] leading to a change in the interatomic distances in thin films. Nevertheless, the increase in T of the γ-Fe_2O_3 film suggests that the Fe-O bonds in γ-Fe_2O_3 are more covalent than those in α-Fe_2O_3, causing the intra-atomic Coulomb energies of Q and U to be screened by the density of polarizable bonds.[27] The increasing covalency could shift the binding energy of the XPS Fe $2p$ levels. This is a second reason for the lowered binding energy of the Fe $2p_{3/2}$ main peak for γ-Fe_2O_3.

The p-d hybridization also influences the satellite positions.[19,21–24,27] The separation between the main and the satellite peaks is approximately given by $\delta E=[(\Delta-Q)^2+4T^2]^{1/2}$. The increase in T of γ-Fe_2O_3 as discussed above makes δE larger, while the decrease in Q makes it smaller when $\Delta<Q$. These two effects cancel each other almost out and the simulated parameters of γ-Fe_2O_3 give a very small decrease in δE for the octahedral Fe^{3+} ions. On the other hand, the spectrum for the tetrahedral Fe^{3+} has satellite positions with larger δE. Therefore, the XPS Fe $2p$ core-level spectrum of γ-Fe_2O_3 contains almost the same satellite positions, but with smaller intensities compared to α-Fe_2O_3.

Figures 6(a) and 7(a) show the observed XPS spectra of the valence-band region of α-Fe_2O_3 and γ-Fe_2O_3 films, respectively. Both spectra consist of a main band (0–10 eV), a satellite band (10–17 eV) and the O $2s$ level (21.5 eV). The main band in both spectra seems to have a three-peak structure with maxima at about 2.7, 4.9, and 7.2 eV, which is in good agreement with the valence-band structures of the corresponding bulk crystals.[2,8] The most remarkable difference between α-Fe_2O_3 and γ-Fe_2O_3 is the intensity of the first peak in the main band at about 2.7 eV. The integrated intensity of the valence-band region (−2.5–17.0 eV) normalized on the O $2s$ intensity is plotted in Fig. 8 for the various iron oxide films. It is noticeable that the valence-band intensity of α-Fe_2O_3 is slightly smaller than that of γ-Fe_2O_3. This should relate in some way to the difference in the number of valence states and suggests a more covalent nature of γ-Fe_2O_3 compared to α-Fe_2O_3. The valence-band spectra are mainly comprised of the Fe $3d$ and the O $2p$ levels. The increased covalency of the Fe^{3+}-O^{2-} bonds should move the electron population from the O $2p$ derived states to the Fe $3d$ derived states. Furthermore, the photoemission cross section of Fe $3d$ is much larger than that of O $2p$.[34] Taking this into account, it is concluded that the Fe-O bonds in γ-Fe_2O_3 are more covalent than those in α-Fe_2O_3, in agreement with the larger Fe $3d$-O $2p$ hybridization as discussed above.

The same parameter values of Δ, T, and U derived from the XPS Fe $2p$ core-level spectra (see Table III) were used for the simulation of the XPS Fe $3d$ valence-band spectra. The effects of the configuration-dependent hybridization,

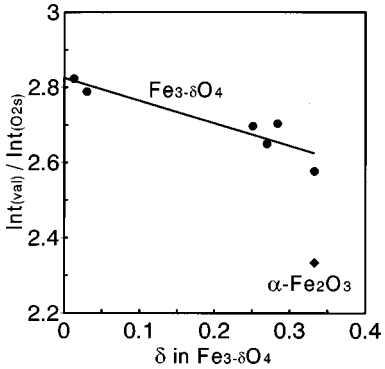

FIG. 8. Integrated valence-band intensities (−2.5–17.0 eV) of various iron oxide films as a function of δ in $Fe_{3-\delta}O_4$. The intensity is normalized on the O $2s$ intensity.

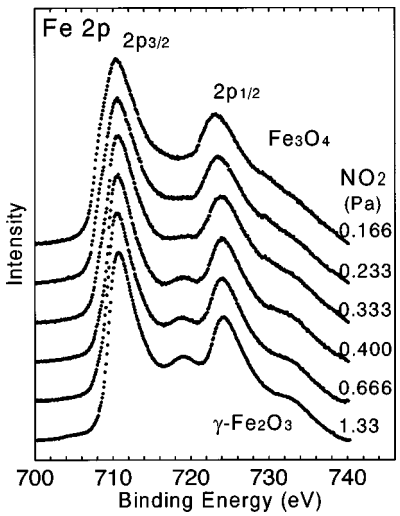

FIG. 9. XPS Fe $2p$ core-level spectra of various iron deficient $Fe_{3-\delta}O_4$ films between γ-Fe_2O_3 and Fe_3O_4 on MgO(100) as a function of the NO_2 pressure during deposition.

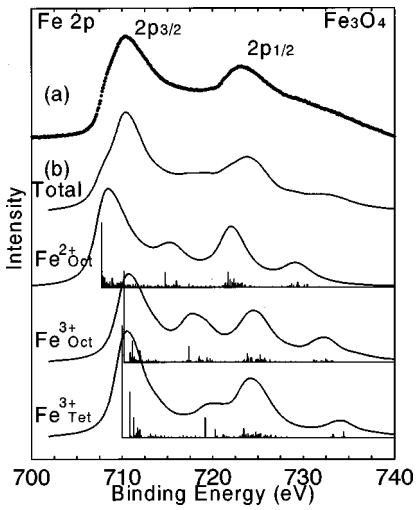

FIG. 10. Observed (a) and simulated (b) XPS Fe $2p$ core-level spectra of a Fe_2O_4(100) film on MgO(100). The simulated spectrum labeled ''Total'' is obtained by a summation of the octahedral Fe^{2+} and Fe^{3+} and the tetrahedral Fe^{3+} components. The parameter values used for the simulation are listed in Table II.

which should bring about a small difference in these parameter values between the XPS Fe $2p$ and $3d$ spectra, were ignored.[35] The simulated spectra shown in Figs. 6(b) and 7(b) reproduce well the satellite structures for both α-Fe_2O_3 and γ-Fe_2O_3 films. It should be noticed again that the Fe $3d$ derived main bands are contaminated by a large contribution from unhybridized O $2p$ states,[6,8] which are left unconsidered in the present calculation. Lad and Henrich reported that the O $2p$ emission exhibited a single broad maximum between 2 and 8 eV, and that the peak shape was essentially identical in each of the various iron oxides.[8] So, the differences in the main band structures between α-Fe_2O_3 and γ-Fe_2O_3 should mainly result from changes in the Fe $3d$ derived states. The calculated spectrum for the tetrahedral Fe^{3+} ions gives a large intensity at lower energies. Thus, we conclude that the tetrahedral Fe^{3+} ions in γ-Fe_2O_3 cause the increase in the first peak intensity of the main band at about 2.7 eV.

B. $Fe_{3-\delta}O_4$ films

Fe_3O_4 is a mixed-valence compound with a conventional notation of $[Fe^{3+}]_{tet}[Fe^{2+}Fe^{3+}]_{oct}O_4$. At room temperature, the octahedral Fe^{3+} and Fe^{2+} ions can formally be written as $Fe^{2.5+}$ because of a rapid electron hopping with a frequency of about 10^{-11} sec.[36] Therefore, the room-temperature Mössbauer spectrum of Fe_3O_4 consists of only two superimposed sextets, assigned to the tetrahedral Fe^{3+} ions and the octahedral $Fe^{2.5+}$ ions, respectively, as shown in Fig. 1(a). However, the core-hole lifetime in the photoemission process is on the order of 10^{-15} sec,[37] which is much faster than the hopping frequency. Therefore, the Fe^{3+} and Fe^{2+} ions in octahedral sites are distinguishable by XPS in contrast to Mössbauer spectroscopy.

Figure 9 shows a series of XPS Fe $2p$ core-level spectra of nonstoichiometric $Fe_{3-\delta}O_4$ films between Fe_3O_4 and γ-Fe_2O_3 as a function of the NO_2 pressure during growth. The film with $\delta=0.013$ prepared at an NO_2 pressure of 0.166 Pa is nearly stoichiometric Fe_3O_4, while the one with $\delta=0.333$ at 1.33 Pa is stoichiometric γ-Fe_2O_3. The intensity of the main-peak shoulder at around 709 eV, which is characteristic for the formation of Fe^{2+} ions,[1–3] increases with decreasing δ. But, in spite of the formation of Fe^{2+} ions, the binding energy of the Fe $2p_{3/2}$ main peak maximum in $Fe_{3-\delta}O_4$ hardly seems to depend on δ. On the other hand, the $2p_{1/2}$ main peak gradually shifts to lower binding energy with decreasing δ. In the XPS spectrum of Fe_3O_4, the $2p_{3/2}$ satellite at about 719 eV characteristic of the Fe^{3+} ions in γ-Fe_2O_3, becomes less resolved due to rising intensities at about 716 eV. These latter intensities are normally assigned to the satellite for the Fe^{2+} ions, analogous to the spectrum of wustite, FeO.[1–3] However, the Fe-O interatomic distance of the octahedral sites in bulk Fe_3O_4 is about 2% smaller than that in bulk FeO.[32] The change in the Fe-O distance should influence the p-d hybridization parameters, as discussed above. To reproduce the XPS Fe $2p$ core-level spectrum for Fe_3O_4 by a cluster calculation, we tried to optimize these parameters for Fe_3O_4. The simulation involved three iron-oxygen clusters, i.e., octahedral Fe^{2+}, octahedral Fe^{3+}, and tetrahedral Fe^{3+} ones.

The simulated XPS Fe $2p$ core-level spectrum of Fe_3O_4, obtained by summation of three spectra of the above clusters, is shown in Fig. 10. The relative binding energies of the Fe^{2+} and the Fe^{3+} spectra were simply determined by subtracting the observed XPS spectrum of γ-Fe_2O_3 from that of Fe_3O_4. The Fe $2p_{3/2}$ main peak maximum of the Fe^{2+} component has a binding energy of 708.5 eV, while that that of the Fe^{3+} components in γ-Fe_2O_3 is 710.6 eV. To optimize the parameter values of Fe_3O_4, we referred to the structural parameters of bulk crystals. The Fe-O interatomic distance of octahedral sites in Fe_3O_4 is enlarged by about 2% compared to γ-Fe_2O_3,[32] which should effect the p-d hybridization parameters. For instance, the Harrison's relations makes T vary with the interatomic distance as $d^{-3.5}$.[29] Furthermore, the intra-atomic Coulomb interactions Q and U are screened mainly due to the polarizability of O^{2-}, which increases with

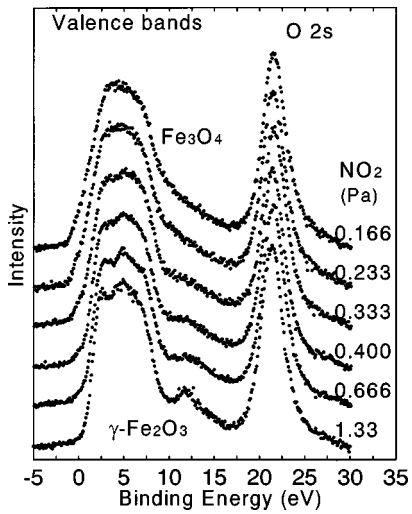

FIG. 11. XPS spectra of the valence-band region of iron deficient $Fe_{3-\delta}O_4$ films between γ-Fe_2O_3 and Fe_3O_4 on MgO(100) as a function of the NO_2 pressure during deposition.

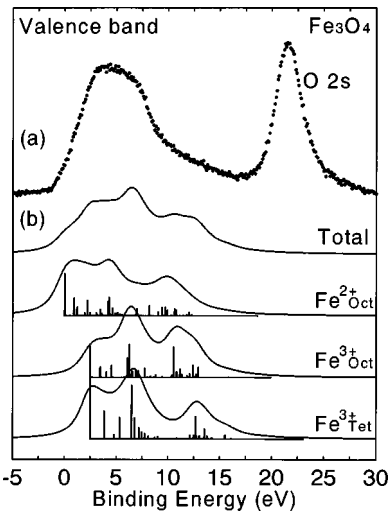

FIG. 12. Observed (a) and simulated (b) XPS spectra of the valence-band region of a Fe_3O_4(100) film on MgO(100). The parameter values measured in the XPS Fe $2p$ spectrum (Fig. 10) are used for the simulation. The simulated spectrum labeled ''Total'' is obtained by the summation of the octahedral Fe^{2+} and Fe^{3+} and the tetrahedral Fe^{3+} components.

decreasing an interatomic distance as r^{-3}.[27] The parameters of the Fe^{2+} ions are expected to have an increase in Δ and T, and a decrease in Q and U compared to those of the Fe^{3+} ions because of the increasing electron densities. On the other hand, the interatomic distance of tetrahedral sites of Fe_3O_4 is slightly decreased in spite of the large increase in unit-cell volume, compared to γ-Fe_2O_3. Thus, the spectrum of the tetrahedral Fe^{3+} in Fe_3O_4 was simulated by using the same hybridization parameters in γ-Fe_2O_3.

Following the above procedure qualitatively, the simulated spectrum for Fe_3O_4 can well reproduce the smeared-out satellite structures between 714 and 720 eV. The broad intensities at about 716 eV can mainly be assigned to the satellite structures of the octahedral Fe^{2+} ions. The satellites in the octahedral Fe^{3+} spectrum also shift their intensities to lower binding energies, but those due to the tetrahedral ions are unchanged. Thus, the unresolved net satellite structures are produced. Unfortunately, our simulation could not reproduce the asymmetric broadening of the Fe $2p$ main peaks very well. This probably results from the larger bandwidth of the XPS final states for Fe_3O_4, reflecting the higher conductivity of this material.[7] According to the ZSA diagram shown in Fig. 5, the Fe^{2+} ions in Fe_3O_4 are plotted in the intermediate regime between the Mott-Hubbard and charge-transfer insulators, just like FeO.[22] However, the higher conductivity in Fe_3O_4, due to the rapid electron hopping, makes the ZSA classification not applicable to this oxide.

Shown in Fig. 11 are the observed XPS spectra of the valence-band region of the $Fe_{3-\delta}O_4$ films as a function of the NO_2 pressure. The integrated intensity of the valence-band peaks in Fig. 8, normalized on the O $2s$ intensity, gradually decreases with increasing δ in $Fe_{3-\delta}O_4$. This result supports the idea that the valence-band intensity is proportional to the number of $3d$ electrons. The spectra have the structures that are strongly dependent on the stoichiometry of the films. With the formation of Fe^{2+} ions, the three-peak structure in the main band becomes unresolved and the intensity at the Fermi level E_F increases. Furthermore, the satellite band gradually shifts its position to lower binding energy with increasing Fe^{2+} content. The Fe^{2+} derived spectrum obtained by subtracting the spectrum of γ-Fe_2O_3 from that of Fe_3O_4 has a main band with a shallow binding-energy level at about 0.83 eV. This intensity near E_F can be related with the conducting nature of the $Fe_{3-\delta}O_4$ films. The simulated XPS Fe $3d$ spectrum shown in Fig. 12(b) was simply obtained by a summation of three spectra of the octahedral Fe^{2+} and Fe^{3+} and the tetrahedral Fe^{3+} ions, similarly to simulate the XPS Fe $2p$ core-level spectrum. The same parameter values of Δ, T, and U derived from the XPS Fe $2p$ spectra were used for the calculation. Although the observed valence-band spectrum is contaminated by unhybridized O $2p$ levels,[8] the simulated spectrum can well reproduce the changes in the structures of the satellite band and the main band with shallow binding energy, going from γ-Fe_2O_3 to Fe_3O_4.

V. CONCLUSION

We reported on a systematic analysis of XPS Fe $2p$ core-level and valence-band spectra of various iron-oxide films prepared by NO_2-assisted MBE. The observed XPS spectra, which were in good agreement with spectra of bulk crystals, were interpreted using cluster-model calculations. The satellite structures in the XPS spectra were caused by the Fe $3d$-O $2p$ hybridization. The XPS Fe $2p$ spectrum of γ-Fe_2O_3 had a smaller satellite intensity compared to α-Fe_2O_3, because of the larger Fe $3d$ to O $2p$ hybridization in γ-Fe_2O_3. Furthermore, the XPS valence-band spectrum of γ-Fe_2O_3, which was comprised of both Fe $3d$ and O $2p$ levels, had a larger normalized intensity than that of α-Fe_2O_3. Both findings indicated an increased covalency of the Fe-O bonds in γ-Fe_2O_3 compared to α-Fe_2O_3. By adjusting the NO_2 pressure during deposition, it was also possible to obtain $Fe_{3-\delta}O_4$ with a precisely controlled stoichiometry.

With the decrease in δ of the $Fe_{3-\delta}O_4$ films from γ-Fe_2O_3 to Fe_3O_4, the XPS spectra showed gradual changes in their structure, mainly because of the formation of Fe^{2+} ions and an increase in the Fe-O interatomic distance of only the octahedral sites but not of the tetrahedral sites. The smeared-out satellite structure of Fe_3O_4 could be reproduced by a summation of three different satellite structures derived from octahedral Fe^{2+}, octahedral Fe^{3+}, and tetrahedral Fe^{3+} ions.

*Present address: Department of Applied Chemistry, Faculty of Engineering, Okayama University, Tsushima-naka 3-1-1, Okayama 700-0082, Japan.

[1] C. R. Brundle, T. J. Chuang, and K. Wandelt, Surf. Sci. **68**, 459 (1977).
[2] N. S. McIntyre and D. G. Zetaruk, Anal. Chem. **49**, 1521 (1977).
[3] P. Mills and J. L. Sullivan, J. Phys. D **16**, 723 (1983).
[4] D. D. Hawn and B. M. DeKoven, Surf. Interface Anal. **10**, 63 (1987).
[5] I. D. Welsh and P. M. A. Sherwood, Phys. Rev. B **40**, 6386 (1989).
[6] A. Fujimori, M. Saeki, N. Kimizuka, M. Taniguchi, and S. Suga, Phys. Rev. B **34**, 7318 (1986).
[7] K. Siratori, S. Suga, M. Taniguchi, K. Soda, S. Kimura, and A. Yanase, J. Phys. Soc. Jpn. **55**, 690 (1986).
[8] R. J. Lad and V. E. Henrich, Phys. Rev. B **39**, 13 478 (1989).
[9] C. Colliex, T. Manoubi, and C. Ortiz, Phys. Rev. B **44**, 11 402 (1991).
[10] Y. Ma, P. D. Johnson, N. Wassdahl, J. Guo, P. Skytt, J. Nordgren, S. D. Kevan, J.-E. Rubensson, T. Böske, and W. Eberhardt, Phys. Rev. B **48**, 2109 (1993).
[11] J. P. Crocombette, M. Pollak, F. Jollet, N. Thromat, and M. Gautier-Soyer, Phys. Rev. B **52**, 3143 (1995).
[12] C. Gleitzer, Key Eng. Mater. **125-126**, 355 (1997).
[13] T. Fujii, M. Takano, R. Katano, Y. Bando, and Y. Isozumi, J. Cryst. Growth **99**, 606 (1990).
[14] D. M. Lind, S. D. Berry, G. Chern, H. Mathias, and L. R. Testardi, Phys. Rev. B **45**, 1838 (1992).
[15] F. C. Voogt, T. Hibma, G. L. Zhang, M. Hoefman, and L. Niesen, Surf. Sci. **331-333**, 1508 (1995).
[16] R. M. Wolf, A. E. M. de Veirman, P. van der Sluis, P. J. van der Zaag, and J. B. F. aan de Stegge, in *Epitaxial Oxide Thin Films and Heterostructures*, edited by D. K. Fork *et al.*, MRS Symposia Proceedings No. 341 (Materials Research Society, Pittsburgh, 1994), p. 23.
[17] Y. J. Kim, Y. Gao, and S. A. Chambers, Surf. Sci. **371**, 358 (1997).
[18] F. C. Voogt, T. Hibma, P. J. M. Smulders, L. Niesen, and T. Fujii, in *Epitaxial Oxide Thin Films III*, edited by C. Foster *et al.*, MRS Symposia Proceedings No. 474 (Materials Research Society, Pittsburgh, 1997), p. 211.
[19] T. Fujii, D. Alders, F. C. Voogt, T. Hibma, B. T. Thole, and G. A. Gawatzky, Surf. Sci. **366**, 579 (1996).
[20] F. C. Voogt, T. Fujii, P. J. M. Smulders, L. Niesen, M. A. James, and T. Hibma (unpublished).
[21] K. Okada and A. Kotani, J. Phys. Soc. Jpn. **61**, 4619 (1992).
[22] A. E. Bocquet, T. Mizokawa, T. Saitoh, H. Namatame, and A. Fujimori, Phys. Rev. B **46**, 3771 (1992).
[23] G.-H. Gweon, J.-G. Park, and S.-J. Oh, Phys. Rev. B **48**, 7825 (1993).
[24] T. Uozumi, K. Okada, A. Kotani, R. Zimmermann, P. Steiner, S. Hüfner, Y. Tezuka, and S. Shin, J. Electron Spectrosc. Relat. Phenom. **83**, 9 (1997).
[25] D. A. Shirley, Phys. Rev. B **5**, 4709 (1972).
[26] J. Zaanen, G. A. Sawatzky, and J. W. Allen, Phys. Rev. Lett. **55**, 418 (1985).
[27] J. van Elp, J. L. Wieland, H. Eskes, P. Kuiper, G. A. Sawatzky, F. M. F. de Groot, and T. S. Turner, Phys. Rev. B **44**, 6090 (1991).
[28] J. C. Slater and G. F. Koster, Phys. Rev. **94**, 1498 (1954).
[29] W. A. Harrison, *Electronic Structure and the Properties of Solids* (Freeman, San Francisco, 1980).
[30] K. Okada, A. Kotani, and B. T. Thole, J. Electron Spectrosc. Relat. Phenom. **58**, 325 (1992).
[31] F. M. F. de Groot, J. Electron Spectrosc. Relat. Phenom. **67**, 529 (1994).
[32] R. W. G. Wyckoff, *Crystal Structures*, 2nd ed. (Wiley, New York, 1967).
[33] T. Fujii, M. Takano, R. Katano, Y. Isozumi, and Y. Bando, J. Magn. Magn. Mater. **135**, 231 (1994).
[34] J. H. Scofield, J. Electron Spectrosc. Relat. Phenom. **8**, 129 (1976).
[35] K. Okada and A. Kotani, J. Electron Spectrosc. Relat. Phenom. **71**, R1 (1995).
[36] B. Balko and G. R. Hoy, Physica B & C **86-88**, 953 (1977).
[37] M. O. Krause and J. H. Oliver, J. Phys. Chem. Ref. Data **8**, 329 (1979).